Journal of
Synchrotron Radiation

ISSN 0909-0495

Received 24 April 2007
Accepted 18 May 2007

A versatile *in situ* spectroscopic cell for fluorescence/transmission EXAFS and X-ray diffraction of heterogeneous catalysts in gas and liquid phase

Stefan Hannemann,[a] Maria Casapu,[a] Jan-Dierk Grunwaldt,[a]* Peter Haider,[a] Philippe Trüssel,[a] Alfons Baiker[a] and Edmund Welter[b]

[a]Department of Chemistry and Applied Biosciences, ETH Zurich, HCI-Hönggerberg, CH-8083 Zürich, Switzerland, and [b]Hamburger Synchrotron Strahlungslabor at Deutsches Elektronen Synchrotron, Notkestrasse 85, D-22607 Hamburg, Germany. E-mail: grunwaldt@chem.ethz.ch

A new spectroscopic cell suitable for the analysis of heterogeneous catalysts by fluorescence EXAFS (extended X-ray absorption fine structure), transmission EXAFS and X-ray diffraction during *in situ* treatments and during catalysis is described. Both gas-phase and liquid-phase reactions can be investigated combined with on-line product analysis performed either by mass spectrometry or infrared spectroscopy. The set-up allows measurements from liquid-nitrogen temperature to 973 K. The catalysts are loaded preferentially as powders, but also as self-supporting wafers. The reaction cell was tested in various case studies demonstrating its flexibility and its wide applicability from model studies at liquid-nitrogen temperature to *operando* studies under realistic reaction conditions. Examples include structural studies during (i) the reduction of alumina-supported noble metal particles prepared by flame-spray pyrolysis and analysis of alloying in bimetallic noble metal particles (0.1%Pt–0.1%Pd/Al_2O_3, 0.1%Pt–0.1%Ru/Al_2O_3, 0.1%Pt–0.1%Rh/Al_2O_3, 0.1%Au–0.1%Pd/Al_2O_3), (ii) reactivation of aged 0.8%Pt–16%BaO–CeO_2 NO_x storage–reduction catalysts including the NO_x storage/reduction cycle, and (iii) alcohol oxidation over gold catalysts (0.6%Au–20%CuO–CeO_2).

Keywords: X-ray absorption spectroscopy; *in situ*; X-ray diffraction; cell design; supported noble metal catalysts; selective catalytic reduction; NO_x storage–reduction catalysts; gold catalysis.

1. Introduction

Synchrotron radiation in the hard X-ray regime has been found to be very effective for studying material structure–property relationships *in situ* (*e.g.* McBreen & Mukerjee, 1995; Iwasawa, 1996; Clausen *et al.*, 1998; Thomas & Sankar, 2001; Grunwaldt & Clausen, 2002; Newton *et al.*, 2002; Topsøe, 2003; Bazin *et al.*, 2003; Russell & Rose, 2004; Barsan *et al.*, 2007, and references therein). Understanding these relationships is of paramount importance in different areas, such as catalysis (structure as function of catalytic performance), solid-state chemistry (structure as function of environmental conditions; properties such as ferroelectricity, ion and electron conductivity, piezoelectricity), sensor technology (structure–gas sensing properties) and electrochemistry (*e.g.* fuel cells). The structure is preferentially identified simultaneously with the material's functional properties because the physical properties are dependent on the atomic structure, which itself varies with the reaction conditions.

In catalysis, crystalline and amorphous high-surface-area materials often occur beside each other. Therefore both X-ray diffraction (XRD) and X-ray absorption spectroscopy (XAS) [in terms of XANES (X-ray absorption near-edge structure) and EXAFS (extended X-ray absorption fine structure)] have been used to determine the structure while measuring the catalytic performance at the same time (Clausen *et al.*, 1991; Thomas & Sankar, 2001; Grunwaldt & Clausen, 2002; Grunwaldt *et al.*, 2004). A number of different cell designs have been proposed (for an overview, see Iwasawa, 1996; Clausen *et al.*, 1998; Thomas & Sankar, 2001; Grunwaldt *et al.*, 2004; Grunwaldt & Baiker, 2007) that consider aspects such as flow dynamics, energy range, signal-to-noise ratio, the spectroscopic techniques to be applied (XAS, small-angle X-ray scattering, XRD), the detection mode in XAS (fluorescence or transmission) and the nature of the surrounding fluid (gas phase, liquid phase, high pressure). For gas-phase reactions, different concepts for *in situ* XAS reaction cells have been proposed. (i) The use of wafers or pressed powders inside a

reaction chamber (*e.g.* Dalla Betta *et al.*, 1984; Lytle *et al.*, 1985; Kampers *et al.*, 1989; Pettiti *et al.*, 1999; Huwe & Fröba, 2004; Longo *et al.*, 2005), which make it possible to probe the catalyst also at liquid-nitrogen temperature. (ii) A cell similar to a plug-flow reactor where the powder is filled into tubes such as quartz capillaries (Clausen *et al.*, 1998; Grunwaldt & Clausen, 2002; Meitzner & Iglesia, 1999) or Be tubes (Bare *et al.*, 2007). This design has also been used for XRD (Clausen *et al.*, 1991; Grunwaldt & Clausen, 2002) and for fluorescence XAS studies (Kappen *et al.*, 2002; Grunwaldt *et al.*, 2005). (iii) A further concept involves the powder catalyst being located between two seals, *e.g.* from Kapton or graphite (Revel *et al.*, 1999; Clausen & Topsøe, 1991; Ressler *et al.*, 2003; Grunwaldt *et al.*, 2004; Girardon *et al.*, 2005). This approach offers the advantage that the probing area is rather large and that the catalyst can be easily filled into the reaction chamber. However, further development is desirable because for this latter concept only a few spectroscopic cell designs have been reported that allow recording XAS spectra both in the transmission and fluorescence mode. In addition, preferentially XRD data should be recorded on the same sample (*cf.* Dent *et al.*, 1992; Clausen *et al.*, 1998; Grunwaldt & Clausen, 2002, for combination of EXAFS and XRD) and studies should be performed both at liquid-nitrogen temperature and at elevated temperature (*i.e.* the reaction temperature). This prompted us to design a new spectroscopic cell. In the reaction cell presented here the powder can be pressed into the holder. A sieved catalyst is used preferentially to ensure good external and internal mass transport. The cell can be cooled with liquid nitrogen and heated to 973 K. The sample thickness and the material of the cell can be varied using insets of different thickness and various reactor materials.

In the first part of the paper, a description of the spectroscopic cell is given. Then various studies on different catalytic systems are presented that demonstrate the application of the cell for fluorescence and transmission EXAFS measurements at different edge energies, the combination with X-ray diffraction, parallel on-line gas analysis, and finally in liquid-phase reactions. The data were recorded at three different conventional XAS beamlines to demonstrate the versatility and the advantages but also the limitations of the presented spectroscopic cell.

2. Experimental

2.1. Overview of the design of the spectroscopic cell for *in situ* catalytic studies

Views of the experimental arrangement and a schematic set-up of the cell are given in Figs. 1 and 2, respectively. The arrangement is divided into the following parts: (*a*) sample stage to align the cell in the X-ray beam (horizontal and vertical adjustment of the stage by Newport motor controllers); (*b*) the body of the *in situ* cell with four windows for the incoming, the transmitted and the diffracted X-rays, and

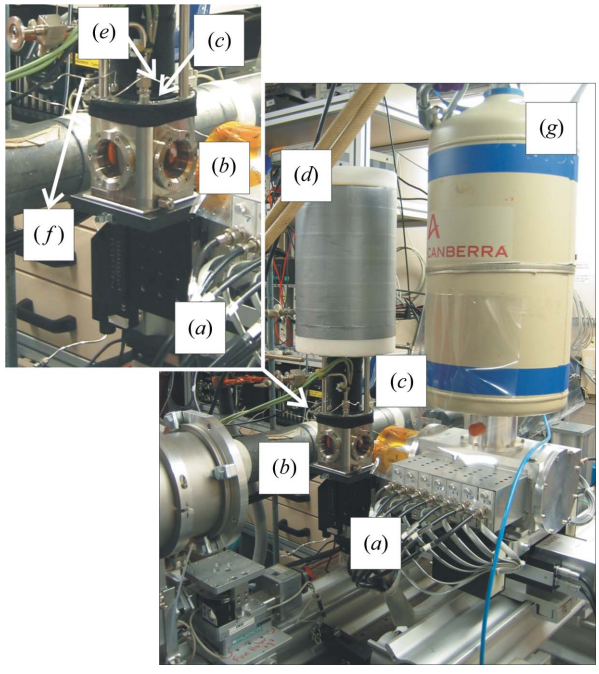

Figure 1
View of the newly designed heatable/coolable *in situ* fluorescence/transmission EXAFS cell (photograph from SNBL at ESRF, Grenoble) with the basic parts highlighted (see text for further details): (*a*) sample stage (Newport); (*b*) body of the *in situ* cell with four windows for incoming, transmitted/diffracted and fluorescence X-rays with an option to be evacuated; (*c*) top part with sample cell, gas inlet and outlet, thermocouples *etc.* (*cf.* Fig. 2); (*d*) liquid-nitrogen container; (*e*) inlet from the reaction gas or liquid supply system; (*f*) outlet to mass spectrometer or infrared spectrometer; (*g*) 13-element Ge detector from SNBL at ESRF. This figure is in colour in the electronic version of the paper.

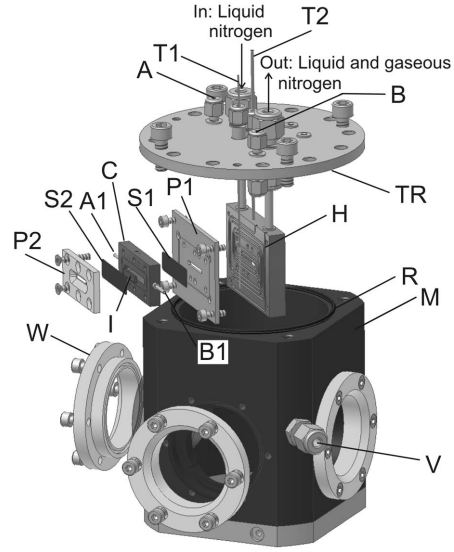

Figure 2
Schematic view of the heatable/coolable *in situ* fluorescence/transmission EXAFS cell also suited to X-ray diffraction. A and A1: gas inlet for the reaction mixture; B and B1: gas outlet of the product gas towards gas analysis; C: reaction cell of stainless steel; H: heat plate with Thermocoax heater and liquid-nitrogen cooling; I: inset; M: main body with Kapton windows (W) and sealings (R) and an outlet to the vacuum pump (V); P1 and P2: plates to assemble the *in situ* cell; S2 and S3: sealing for the *in situ* cell; T1 and T2: thermocouples [a Teflon ring (TR) is optionally used, see text].

windows for recording fluorescence X-rays perpendicular to the beam [fluorescence detector (*g*), on both sides possible, depending on the design of the beamline] including a vacuum flange assuring thermal insulation; (*c*) the top/inner part of the cell with heater, liquid-nitrogen cooling and the sample compartment with gas inlet/outlet (see Fig. 2 for a magnification of the top part of the main body); (*d*) the thermally insulated liquid-nitrogen container; (*e*) the gas or liquid supply system (only schematically drawn) and (*f*) an on-line mass spectrometer or infrared spectrometer for product analysis (schematically indicated). The reaction cell, which is mounted on (*c*) and which is described in more detail in the next section, was designed in a way that the sample compartment including heating is as small as possible to achieve a rather local heating. This prevents the main cell body from being heated to >423 K, even if the reaction cell itself is at a temperature of 973 K. Note that no evacuation of the body is required during heating and if the samples are measured at low edge energies the volume can be flushed with helium. The Kapton windows (Fig. 2, W) and the O-rings (Viton), that are used to seal the body of the cell (*b*) from the environment, can further withstand temperatures >473 K. More critical is cooling with liquid nitrogen. In this case the body of the cell (*b*) has to be evacuated to prevent ice formation on the windows. In addition, optionally a Teflon-ring (TR, inner diameter 70 mm, outer diameter 110 mm, thickness 0.5 or 1 mm) between the top part (*c*) with the reaction cell and the main body (*b*) was placed to thermally decouple the upper part from the lower part. During longer cooling (>1 h) with liquid nitrogen the windows were flushed with compressed air to prevent the condensation of water. The construction of the liquid-nitrogen container (*d*) in Fig. 1 is similar to the one reported by Kampers *et al.* (1989). It consists of a stainless steel container surrounded by insulation material (PIR polyisocyanate foam for thermal insulation around the container and the base and top plate of Rohacel foam). Two tubings (inner diameter of 8 mm) make it possible to feed the liquid nitrogen into the sample holder (H, Fig. 2) and let it flow out together with gaseous nitrogen.

2.2. Reaction cell including heating/cooling plate

The heart of the cell is the top part of the main body (*c*) in Fig. 1 with the sample holder and reaction cell that can be removed for loading the sample as shown in Fig. 2. A more detailed view of the sample holder itself is provided in Fig. 3, showing the cell from the top and the X-ray path through the centre of the reaction cell. Note that the capital letters refer to both Figs. 2 and 3. In brief, it consists of a heatable/coolable stainless steel holder (H), a plate (P1) with a sealing/window S1, which are mounted onto the holder, the reaction cell (C) and a plate (P2) with a sealing/window S1 on top. The holder (H) contains a thermocouple (T2), the heating and the cooling system. As depicted in Figs. 2 and 3(*a*), channels for embedding the Thermocoax heater (Thermocontrol GmbH) are present in the heating plate (H, on the left). The liquid-nitrogen loop for cooling is incorporated in the middle of the plate. For controlling the temperature of the heater an appropriate controller (KS20-I, PMA Process- und Maschinen-Automation GmbH) with optimized PID parameters was applied. In the middle, the holder (H) contains a 17 mm × 3 mm hole for the transmission of the X-rays and also for X-ray diffraction (therefore the hole widens towards the back, *cf.* Fig. 3). The base plate P1 is required because two screws (Fig. 3, Sc1) are needed to fix the reaction cell C onto this plate and to exchange sealings from experiment to experiment. Note that these two screws are only required to mount the reaction cell C onto the plate P1. Then this assembly is fixed with four screws (Sc2) onto the holder H. After filling the cell with powder, a second sealing S2 is placed onto the reaction cell and the plate P2 is fixed with six screws (Sc3). Proper and uniform screwing using a torque spanner is crucial since the six screws fix the plates properly onto the reaction cell (C) and the holder (H). The X-ray transmittant sealings which simultaneously serve as windows were 9 mm × 32 mm in size. Usually, graphite, as proposed earlier by Revel *et al.* (1999) and Girardon *et al.* (2005), Kapton and aluminium

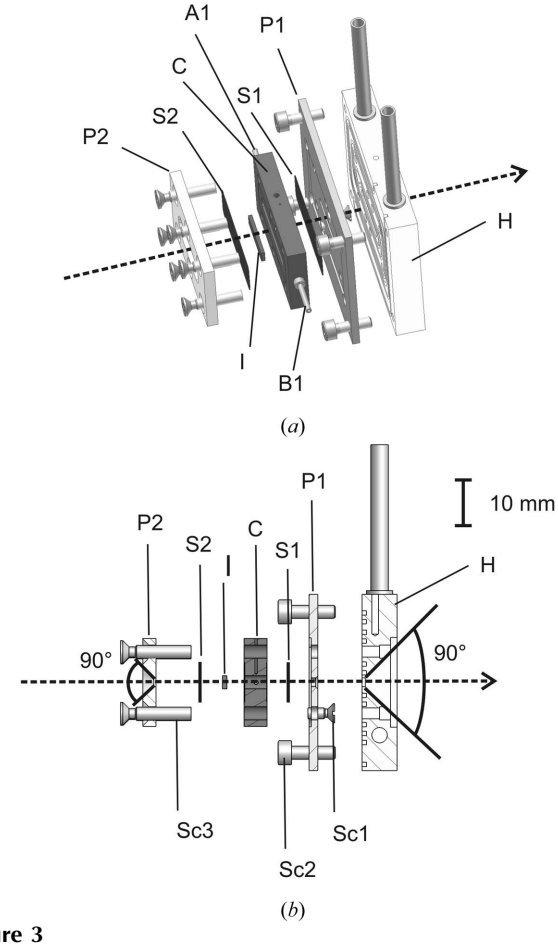

Figure 3
The sample holder H and reaction cell C with the path of the X-ray beam: (*a*) three-dimensional schematics from the top; (*b*) cross section through the centre of the *in situ* cell (the angles show the opening angle of the plate P2 and the heater H, which are required for the fluorescence XAS and the powder diffraction data); notation like in Fig. 2; in addition, the screws (Sc1 to Sc3) to mount the cell are depicted.

foil were used. All the sealings/window materials were self-made by punching with an appropriate template.

This modular set-up allows us to vary the construction material and dimensions (volume) of the reaction cell C. Mainly, its thickness was varied between 1 and 5 mm to adjust for the energy range to be measured and for the X-ray attenuation/matrix of the sample. In its basic design made of stainless steel, the thickness was 2 mm and the dimensions of the sample compartment were 26 mm × 3 mm. Before filling the sieved powder into the cell, a glass-wool plug was positioned on both sides of the sample compartment. The gas inlet in Fig. 2 is from the back (A1) and the outlet in front (B2), which is directly connected to the holder (denoted A and B in Fig. 2) *via* 1/16" tubings. The temperature of the reaction cell was measured from the top (thermocouple T1). As outlined above, the cell volume can be reduced either by varying the reaction cell C or by using an inset. One inset (with a 14 mm × 2 mm hole) has been constructed to minimize the sample volume. In most cases, sieved powder (100–200 µm) was used to ensure optimal mass transfer during the reaction. Since the gas-flow characteristics are similar to a conventional laboratory plug-flow reactor, a mass spectrometer in gas-phase reactions and an infrared spectrometer in liquid-phase reactions were used to acquire kinetic data during the XAS measurements (*cf.* §2.4). Alternatively, a self-supporting wafer can be applied by just pressing the powder into the holder.

Fig. 3(*b*) shows the resulting X-ray path through the cell in transmission mode. Note also the opening angle of 90° in the heating plate serving as sample holder (H) which allows X-ray patterns to be recorded behind the sample. The same is valid for the front plate (P2) so that all fluorescence X-rays in a reasonable angle can be collected in the fluorescence XAS mode.

After the reaction cell (C) including the windows (sealings), the plates (P1) and (P2) are mounted on the sample holder (H), the gas inlet and outlet are connected, and the top part (*c*) with sample cell is fixed onto the base holder (*b*) and the stage (*a*; *cf.* Fig. 1). The assembly (*c*) can be mounted at 90° (only for transmission XAS and XRD), 45° and 30° (also fluorescence mode possible) to the beam and is tightened by an O-ring (Viton).

2.3. XAFS and XRD measurements

The cell has been successfully applied in various studies recorded under different conditions at the following beamlines: at ANKA-XAS (Forschungszentrum Karlsruhe), fluorescence and transmission XAS data were recorded; at beamline X1 at HASYLAB (DESY, Hamburg), XAS data in fluorescence and transmission mode were combined with XRD; and at SNBL at ESRF, fluorescence and transmission XAS spectra were recorded at $E > 20$ keV. In all cases a Si(111) double-crystal monochromator was used for monochromatization of the X-ray intensity and ionization chambers were used for recording the incoming and transmitted intensity. Only for acquisition of XAS spectra at the Ba *K*-edge and the corresponding XRD patterns was a Si(311) double crystal chosen (beamline X1 at HASYLAB).

At ANKA-XAS, transmission and fluorescence spectra on alumina-supported noble metal particles were recorded at the Pt L_3-edge. For fluorescence XAS measurements, a five-element Ge solid-state detector (Canberra) was applied. Data acquisition was performed as reported in earlier studies using another *in situ* cell (Grunwaldt *et al.*, 2005; Hannemann *et al.*, 2006).

Experiments at HASYLAB were performed with a seven-element Si(Li) detector (7-SSD, Gresham) both on 0.8%Pt–16%BaO–CeO_2 and 0.6wt%Au–20wt%Cu–CeO_2 catalysts to determine the structure of the Pt and Au nanoparticles in the same way as described for the ANKA-XAS studies. Aluminium foil as filter was used in both cases to minimize the fluorescence of the matrix (stemming mainly from ceria, barium and copper). In addition, XRD measurements on the 0.8%Pt–16%BaO–CeO_2 catalyst including transmission XAS at the Ba *K*-edge were performed. Fig. 4 depicts schematically this set-up and shows a photograph of the cell in operation at

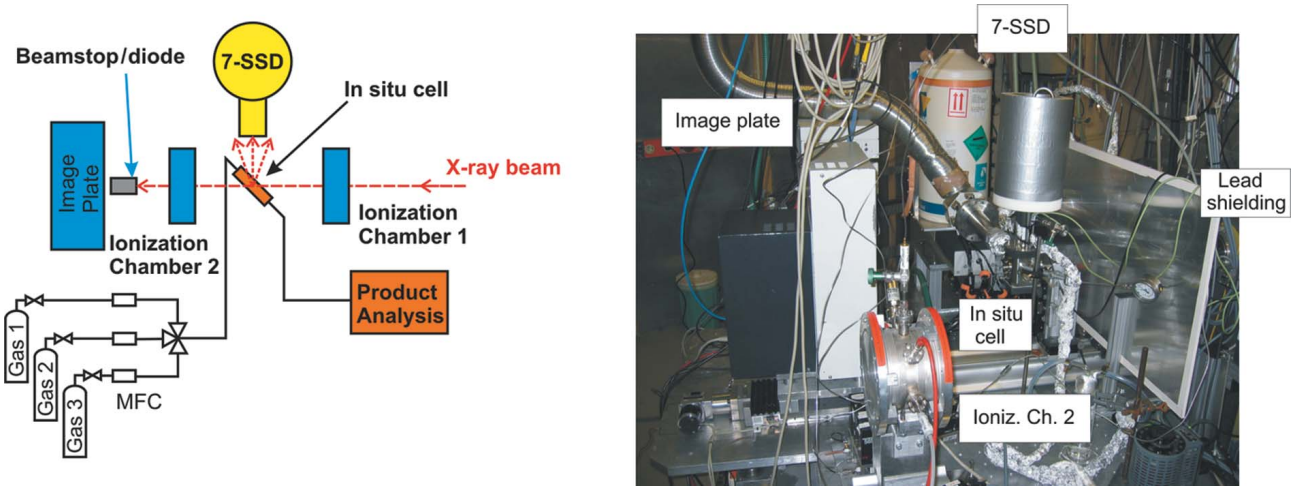

Figure 4
Experimental set-up for the combined fluorescence EXAFS, transmission EXAFS and XRD experiment at HASYLAB (see text for details). This figure is in colour in the electronic version of the paper.

Table 1
Overview of the samples, their preparation and the reactions carried out in the present study.

System	Chapter	Catalyst	Preparation method	Reference to preparation	Reactions performed
Bimetallic noble metal catalysts	3.1	0.1%Pt–0.1%Pd/Al_2O_3 0.1%Pt–0.1%Ru/Al_2O_3 0.1%Pt–0.1%Rh/Al_2O_3 0.1%Au–0.1%Pd/Al_2O_3	Flame synthesis	Hannemann *et al.* (2007)	Reduction in 5%H_2/He
Palladium supported on $LaCoO_3$ perovskite	3.1	0.5%Pd/$LaCoO_3$	Flame synthesis	Chiarello *et al.* (2007)	Reduction in 5%H_2/He; during SCR
NO_x storage–reduction catalyst	3.2	0.8%Pt–16%BaO–CeO_2	Impregnation	Casapu *et al.* (2006)	Reactivation of aged catalyst and NO_x storage–reduction steps
Supported gold catalyst	3.3	0.6%Au–20%CuO–CeO_2	Deposition of Au on flame-synthesized CuO–CeO_2	Haider *et al.* (2007)	Alcohol oxidation in toluene

HASYLAB with the fluorescence detector (7-SSD) on the back and a two-dimensional area detector (MAR 345 image plate) for recording X-ray patterns behind the sample. The active area of the image plate has a diameter of 345 mm. It was positioned 486 mm behind the sample with the incoming beam aimed at the center of the image plate. The range behind the sample covered by the image plate was 39° (a 2θ range of 19.5°).

The beamstop consists of an Al tube with an inner diameter of 2 cm. The back is closed by 1 mm Al and 3 mm Pb plates. The Pb acts as an actual beamstop while the Al absorbs the Pb *L*-fluorescence lines. A quadratic (1 cm edge length) Hamamatsu pin-diode is installed in the tube for recording the transmitted X-ray intensity. The entrance window of the Al housing is made of black non-transparent Kapton foil. This arrangement offers the advantage that both EXAFS and XRD data could be recorded in parallel. Alternatively, a second ionization chamber could be manually installed between the cell and the image plate. Usually, this insertion of the ionization chamber was not the time-limiting step since the image plate had to be read out after irradiation, requiring 30–90 s depending on the number of pixels. In front of the sample cell a large lead plate was placed (*cf.* Fig. 4) to minimize the scattered high-energy X-ray background originating from the monochromator tank on the image-plate detector. The first ionization chamber was placed in front of the lead shielding (therefore not visible in Fig. 4).

The experiment at SNBL was similar to those reported at the HASYLAB and ANKA facilities. In this case a 13-element Ge solid-state detector (Canberra) was applied with corresponding electronics (*cf.* Rohr *et al.*, 2005) and, like for the other fluorescence detectors, software SCAs (single-channel analyzers) were used to record the intensity of the fluorescence lines of interest as a function of the incoming energy. The measurements presented in this study were mainly performed on the systems given in entry 1 in Table 1 and on 0.5%Pd/$LaCoO_3$. To minimize the fluorescence from the matrix, aluminium and chromium filters were added.

All XANES and EXAFS spectra were analysed using the *WINXAS3.1* software (Ressler, 1998). The raw data were energy calibrated, background corrected and normalized. The Fourier transformations for EXAFS spectra were applied to the k^3-weighted functions and were fitted in *R*-space. Phase shifts and backscattering amplitudes for the bimetallic noble metal particles were calculated using *FEFF6.0* (Zabinsky *et al.*, 1995). Deviations of the distances were within ± 0.02 Å, and those for the coordination numbers were within ± 0.5.

The XRD patterns were extracted using the software *FIT2D* (Hammersley, 2007; Hammersley *et al.*, 1994). The whole area of the detector was integrated after a proper fitting of the centre of the beam and correction of the tilt. Powder diffraction patterns were simulated using data from the Inorganic Crystal Structure Data (ICSD) database. The distances to the detector and the angles were calibrated using LaB_6 as a standard.

2.4. Catalytic experiment and catalyst samples

Table 1 gives an overview of the investigated samples, a reference to the corresponding preparation route, and the reactions that are the focus of the present paper. Further details are described in the corresponding section of the case study. Except for the last reaction in Table 1 (alcohol oxidation over 0.6%Au–20%CuO–CeO_2), all catalysts were investigated in the gas phase. The gas feed in the gas-phase reactions was controlled by three mass-flow controllers (Brooks, 0–50 ml min^{-1}, *cf.* schematic drawing in Fig. 4). Typically, pre-mixed gases were fed through the *in situ* cell and one of the gas feeds could be saturated with water at room temperature (*cf.* NO_x storage–reduction catalysts). A mass spectrometer (Balzers Thermostar) served for the analysis of the effluent of the reactor cell, that is, for the analysis of evolving products during temperature-programmed reduction/oxidation and catalytic experiments. The measurements of the catalysts in fluorescence mode during the liquid-phase reactions were performed using the same type of reaction cell as for gas–solid reactions and the catalytic experiment was similar to previous transmission EXAFS experiments (Grunwaldt *et al.*, 2003, 2006). Also, in this case the spectroscopic cell served as a continuous-flow reactor, here for alcohol oxidation over the gold-based catalyst. The solvent toluene including the reactant 1-phenylethanol was introduced using a peristaltic pump (ISMATEC ISM827). The liquids were saturated with Ar and O_2, respectively, and fed into the spectroscopic cell at a flow rate of about 0.3 ml min^{-1}. An IR spectrometer (BRUKER Tensor27, equipped with a DTGS detector) with a transmis-

sion IR cell was placed next to the exit of the spectroscopic cell to trace the conversion on-line. The infrared spectrometer was positioned as close as possible to the EXAFS cell to minimize the dead volume.

3. Case studies

3.1. Flame-made monometallic and bimetallic noble metal catalysts

To demonstrate the capability of the *in situ* XAS cell for fluorescence XAS measurements and *in situ* studies, as a first example the reduction of bimetallic noble metal catalysts prepared by flame synthesis (Table 1, entry 1) is presented. As listed in Table 1, all catalysts contained 0.1% Pt or 0.1% Au together with 0.1% Pd, 0.1% Rh or 0.1% Ru. The catalysts were prepared by flame-spray pyrolysis (Strobel *et al.*, 2006) and, as in the case of higher-loaded corresponding catalysts, the noble metals were in an oxidized state (Strobel *et al.*, 2005; Hannemann *et al.*, 2007). Therefore, in order to study possible alloy formation, the catalysts were first reduced by heating in 5%H_2/He and then investigated at room temperature and close to liquid-nitrogen temperature.

Fig. 5 shows XANES spectra at the Pt L_3-edge during the reduction of the flame-made 0.1%Pt–0.1%Pd/Al_2O_3 taken in fluorescence mode (five-element Ge solid-state detector at ANKA-XAS). Obviously the catalyst remains in an oxidized state when heating in 5%H_2/He up to 473 K. Higher-loaded Pt–Pd/Al_2O_3 is typically reduced already at <423 K (Hannemann *et al.*, 2007) and this shift to elevated temperature is attributed to the low noble metal concentrations and the high dispersion of the noble metals (Stark *et al.*, 2005). After complete reduction, the catalyst was cooled down under the same atmosphere to ~123 K and analysed both in transmission and fluorescence mode. As depicted in Fig. 6, the data quality is improved in fluorescence compared with transmission detection. Furthermore, data fitting of the Fourier-transformed spectra proved that Pt and Pd are alloyed (Table 2). Alloy formation is also reflected by the peaks at 1.8 and 2.2 Å in the Fourier-transformed spectrum (Hannemann *et al.*, 2006). The combination of 0.1% Pt with 0.1% Pd was extended to the systems 0.1%Pt–0.1%Rh, 0.1%Pt–0.1%Ru as well as 0.1%Au–0.1%Pd each supported on alumina (Table 1). As Table 2 shows, for all reduced catalysts a rather small particle size (total coordination number ≪12) and, for the

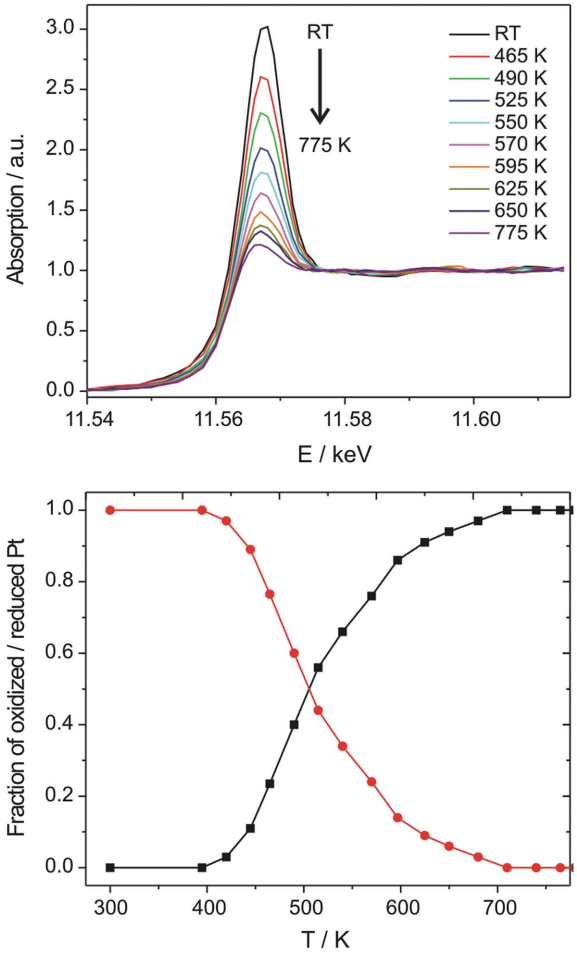

Figure 5
Fluorescence XANES spectra during the reduction of a 0.1%Pt–0.1%Pd/Al_2O_3 catalyst including the corresponding linear combination of the spectra showing the decrease of the oxidized Pt species and the increase of metallic Pt. This figure is in colour in the electronic version of the paper.

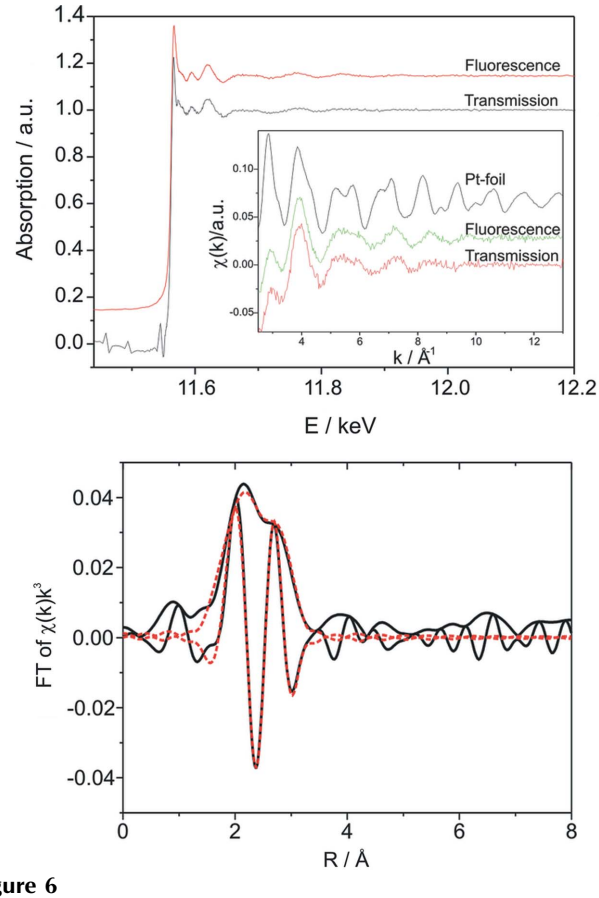

Figure 6
Comparison of fluorescence and transmission EXAFS data and the k^3-weighted Fourier transform of the fluorescence EXAFS data including the best two-shell fit (*cf.* Table 2). This figure is in colour in the electronic version of the paper.

Table 2
Structural parameters of flame-made alumina-supported materials determined by the fitting of Fourier-transformed EXAFS spectra at the Pt L_3-edge (after *in situ* reduction in 5% H_2/He).

A: absorber atom; Bs: backscatter atom; *r* distance; CN: coordination number; σ^2: Debye–Waller factor, set to the same value for both shells; Residual: quality of fit according to Ressler (1998).

Material	A—Bs	*r* (Å)	CN	σ^2 (Å^2)	Residual
0.1%Pt–0.1%Pd	Pt—Pt	2.84	3	0.004	3
	Pt—Pd	2.84	5	0.004	
0.1%Pt–0.1%Rh	Pt—Pt	2.66	3	0.008	5
	Pt—Rh	2.66	1	0.008	
0.1%Pt–0.1%Ru	Pt—Pt	2.67	8	0.008	7
	Pt—Ru	2.67	2	0.008	
0.1%Au–0.1%Pd	Au—Au	2.77	4	0.005	3
	Au—Pd	2.77	2	0.005	

Pt–Pd, Pt–Ru and Au–Pd systems, alloying was found. Additional evidence for alloying arises from data at the corresponding Pd *K*- and Ru *K*-edges (not shown).

Only in the case of the 0.1%Pt–0.1%Rh/Al_2O_3 catalyst was a weaker alloying found indicated by the ratio of coordination numbers of CN(Pt–Pt):CN(Pt–Rh) = 3:1. In fact, a tendency to segregation of Pt and Rh is in line with predictions from computational studies (Ruban *et al.*, 1999) and it seems that, despite the small particle size and the low concentration, alloy formation occurs in a similar way as for higher-loaded samples. With respect to the cell, the study shows that fluorescence and transmission XAS data can be collected simultaneously on powdered materials *in situ* and at low temperature. Further studies have been performed using these alloyed systems in the field of partial oxidation of methane to hydrogen and carbon monoxide as well as the total oxidation of hydrocarbons (Strobel *et al.*, 2005; Hannemann *et al.*, 2007). Recently, these studies were extended to the identification of Pd in flame-synthesized 0.5%Pd/$LaCoO_3$ (studies performed at SNBL using the set-up presented in Fig. 1). These materials are promising for NO_x removal and combustion of hydrocarbons (Kucharczyk & Tylus, 2004; Engelmann-Pirez *et al.*, 2005). Similar to the bimetallic alloys, the structure of Pd could be identified during reduction in 5%H_2/He and reaction in 0.25%NO/1%H_2/5%O_2/He (details will be presented by Chiarello *et al.*, 2007). This demonstrates the applicability of the cell at other absorption beamlines, under reaction conditions (here, selective catalytic reduction) and the extension to higher energies and more strongly X-ray absorbing supports, which will be underlined in the following sections.

3.2. Pt–Ba–CeO_2 NO_x storage–reduction catalysts

3.2.1. Reactivation of a thermally aged Pt/Ba/CeO_2 catalyst. In a next step, the cell was tested over a course of studies on NO_x storage–reduction (NSR) catalysts. Recently, we investigated the thermal deactivation of Pt/Ba/CeO_2 catalysts due to the formation of $BaCeO_3$ in air at temperatures above 973 K (Casapu *et al.*, 2006). Moreover, we found that $BaCeO_3$ in a thermally aged Pt/Ba/CeO_2 catalyst can be decomposed under certain process conditions, *e.g.* in the presence of NO_2, H_2O and CO_2. However, preferentially the studies of catalyst reactivation should be performed *in situ* since both water and CO_2 present in the air influence the surface properties of the catalyst. Here, the cell was utilized with an aged Pt(1 g)/Ba(20 g)/CeO_2 (100 g) sample (denoted 0.8%Pt–16%BaO–CeO_2, *cf.* Table 1).

The newly designed spectroscopic cell is well suited to the investigation of this catalyst system since XANES spectra at the Pt L_3-edge can be acquired in the fluorescence mode (Fig. 7*b*), XAS spectra at the Ba *K*-edge in transmission (Fig. 7*a*) and XRD patterns using the image plate (Fig. 7*c*) resulting in the XRD pattern given in Fig. 7(*d*). The XAS spectra and the X-ray patterns were recorded at beamline X1 (HASYLAB) with the experimental arrangement as depicted in Fig. 4. Note that the XAS spectrum at the Ba *K*-edge was recorded with the pin-diode and the XRD pattern was taken below the Ba *K*-edge at 0.332 Å (37.4 keV). The XRD patterns were extracted using the software *FIT2D* by correcting both for the centre and a possible tilt (*cf.* §2.3).

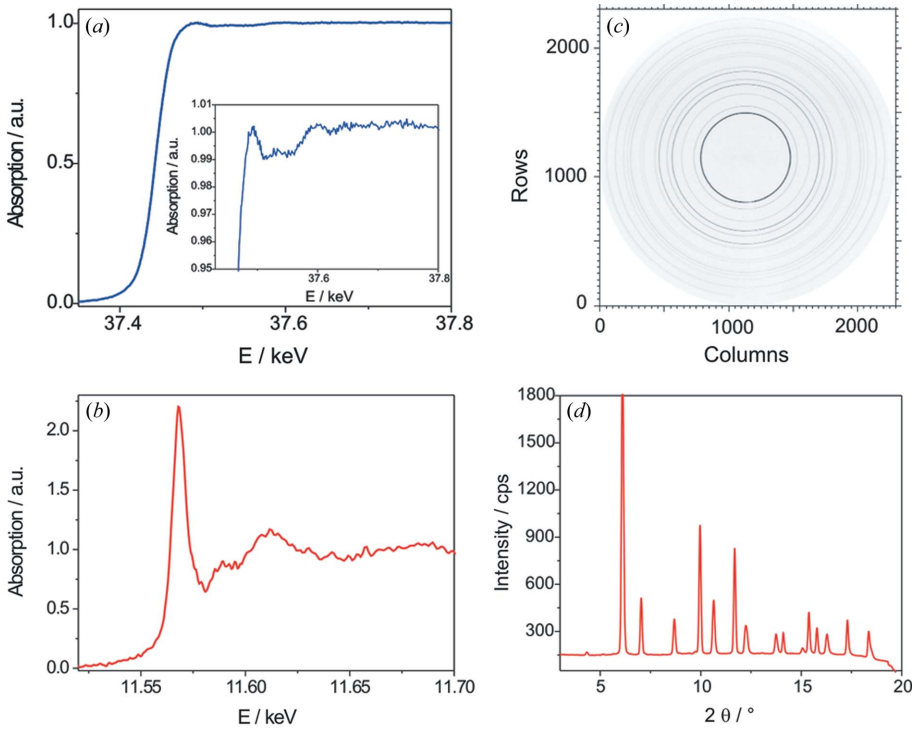

Figure 7
Analysis of the thermally aged 0.8%Pt–16%BaO–CeO_2 (calcined for 10 h at 1273 K) in the *in situ* cell: (*a*) transmission EXAFS spectrum at the Ba *K*-edge, (*b*) fluorescence EXAFS spectrum at the Pt L_3-edge, (*c*) diffraction pattern recorded with an image plate and (*d*) the integrated X-ray pattern. This figure is in colour in the electronic version of the paper.

Both the XAS spectra and the XRD pattern recorded for the aged Pt/Ba/CeO_2 catalyst show the presence of $BaCeO_3$ and a highly oxidized state of the Pt component. As known from previous studies, the presence of $BaCeO_3$ deteriorates the NO_x storage–reduction properties of the catalyst, but it can be reactivated in an NO_2/H_2O atmosphere (Casapu *et al.*, 2007). In order to further understand the reactivation process of the aged catalyst by the decomposition of $BaCeO_3$ in the presence of NO_2/H_2O, XRD patterns were recorded at 673 K under a continuous gas flow of 50 ml min^{-1} (Fig. 8). The data obtained support our previous observation that $BaCeO_3$ is decomposed, which is therefore an interesting option to reactivate aged NSR catalysts. The transformation occurred during a time interval of less than 2 h between 1:40 and 3:20 h after commencing the reaction. $BaCeO_3$ is directly transformed to $Ba(NO_3)_2$. In parallel, *in situ* XAS data at the Ba *K*-edge were obtained, which indicate that a transformation of X-ray amorphous phases of $BaCeO_3$ may occur first.

3.2.2. Oxidation state of Pt during NO_x storage and reduction process in Pt/Ba/CeO_2 catalyst. Whereas the Pt oxidation state did not change upon reactivation, strong changes of the oxidation state are expected during the NO_x storage and reduction process (Anderson *et al.*, 2003). Thus the cell was also used for *in situ* fluorescence XAS measurements at the Pt L_3-edge during exposure of Pt/Ba/CeO_2 catalyst for 30 min at 573 K to a gas flow of 35 ml min^{-1} consisting of a mixture of 0.5%NO/He and 21%O_2/He and later to 2.5%C_3H_6/Ar. XAS spectra were taken every 5 min. Prior to the experiment the sample was heated to 773 K in an inert atmosphere at a rate of 10 K min^{-1} to remove all physisorbed species and then cooled down to the reaction temperature. If, at the beginning of the NO_x storage–reduction process, Pt is in a metallic state (Fig. 9, top), a variation of the oxidation state during the NO_x storage and reduction process was observed. As Fig. 9 shows, Pt is partially reoxidized during the NO_x storage step and it is rapidly and completely reduced again during the reduction step, here performed using propene (Fig. 9, bottom). The XANES spectra allow the estimation of the oxidation state using appropriate references and thus give insight into the dynamic behaviour of the catalyst system.

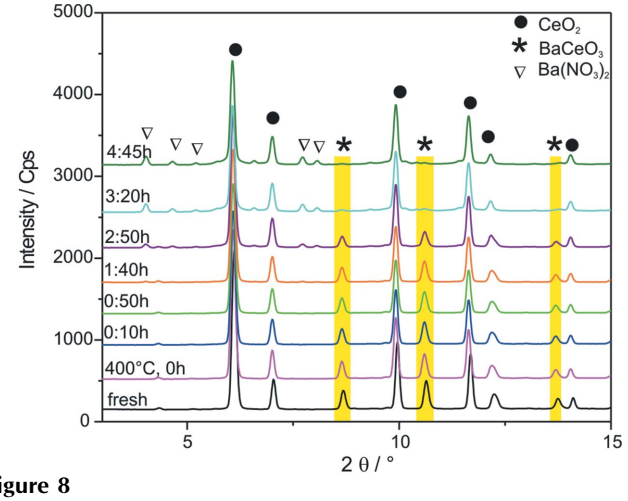

Figure 8
In situ XRD data recorded during the reactivation of the thermally aged 0.8%Pt–16%BaO–CeO_2 catalyst (freshly calcined for 10 h at 1273 K) in 0.5%NO_2–1.5%H_2O–10%O_2/He in the *in situ* cell (shaded areas emphasize the disappearance of $BaCeO_3$ during the course of the reaction). This figure is in colour in the electronic version of the paper.

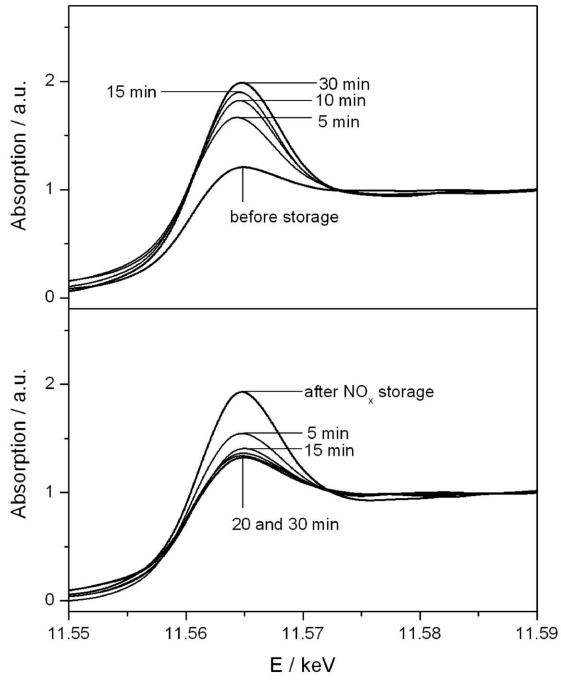

Figure 9
In situ XAS measurements during the NO_x storage (top) and reduction (bottom, with propene) process on the 0.8%Pt–16%BaO–CeO_2 catalyst; the corresponding time is added to the graphics.

3.3. Fluorescence XAS data in the liquid phase during alcohol oxidation over Au/CeO_2

In analogy with the experiments in the gas phase, the spectroscopic cell can also be applied in the liquid phase. One of the reactions in our present focus is alcohol oxidation over noble metal catalyst. Recently, gold has attracted a lot of attention in a number of oxidation and reduction reactions (see reviews by Haruta & Daté, 2001 and Bond & Thompson, 1999) including alcohol oxidation. Similarly, as in the case of Pd catalysts (Keresszegi *et al.*, 2003; Grunwaldt *et al.*, 2006), there is an intensive discussion concerning the oxidation state of gold under reaction conditions (Abad *et al.*, 2005; Onal *et al.*, 2004). Therefore different gold-based catalysts were subject to the present study. For deriving structure–activity relationships both the structure (using XAS) and the catalytic activity using an infrared spectrometer [similar to transmission XAS studies by Grunwaldt *et al.* (2006)] were analysed simultaneously. Fig. 10 shows XAS and IR data collected over a 0.6wt%Au/CuO–CeO_2 catalyst prepared by deposition precipitation. During heating of the catalyst to 353 K in Ar-saturated toluene, no changes of the oxidation state of gold occurred and the gold particles remained in a partially oxidized state. However, when the catalyst was exposed to the reaction mixture of 20 m*M* 1-phenylethanol in toluene satu-

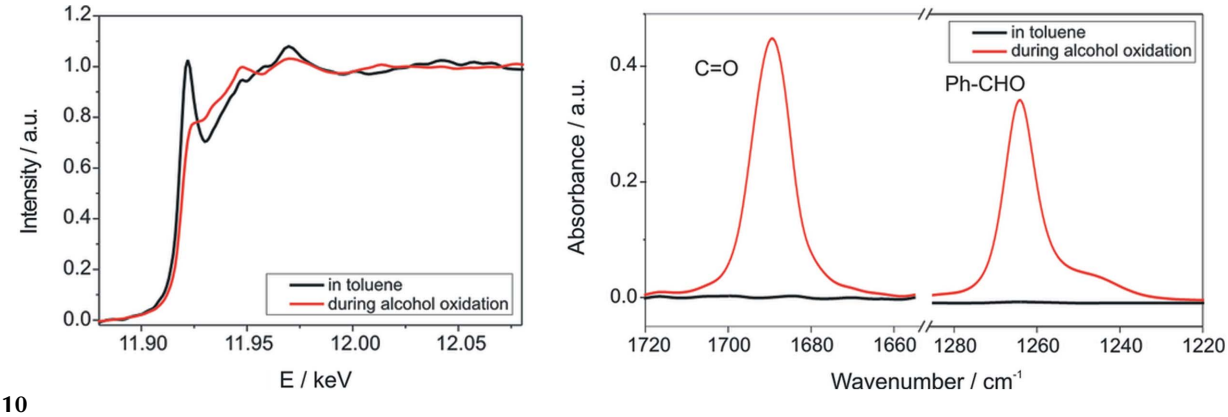

Figure 10
In situ XAS measurements at 353 K of the as-prepared 0.6%Au–20%CuO–CeO_2 catalyst in Ar-saturated toluene and under reaction conditions in oxygen-saturated 1-phenylethanol/toluene with the corresponding on-line catalytic data traced by on-line Fourier-transform IR spectroscopy (see text for details). This figure is in colour in the electronic version of the paper.

rated with O_2, a rapid reduction of Au on 0.6wt%Au/CuO–CeO_2 occurred resulting in the formation of zero-valent Au species. A high rate of ketone (acetophenone) formation was observed [indicated by the two characteristic bands at 1690 cm^{-1}, the ν(C═O) vibration in acetophenone, and 1263 cm^{-1}, ν(C—CO) of the ring and the carbonyl C in Fig. 10 chosen for the product quantification], accompanied by a slight activation of the catalysts. Combined with further results on additional supported gold catalysts, this indicates that zero-valent Au is the catalytically active species (Haider *et al.*, 2007). The results show that the cell can be used in the same way for *in situ* XAS measurements in the transmission and fluorescence mode in the liquid phase as reported in §3.1 and §3.2 for gas-phase reactions. In both cases, on-line determination of the catalytic activity can be achieved allowing the description of structure–activity relationships.

4. Discussion and conclusion

We have presented a new spectroscopic cell for *in situ* XANES and EXAFS, in both the transmission and fluorescence mode, as well as XRD (preferentially $\lambda < 1$ Å). The three case studies show the application of the cell at low metal concentrations, during dynamic changes of the gas conditions as well as under static conditions. A special feature of the cell is its compatibility to both low temperatures (by liquid nitrogen) and high reaction temperatures (up to 973 K) covering most of the needs for spectroscopic studies in catalysis. Owing to the fact that different sealings can be utilized, the cell can be applied for various elements, principally down to the S *K*-edge. Recently it was used at the V *K*-edge using different vanadia-doped catalysts. Only the application of XRD at low energies is restricted since the 2θ scale is fixed up to 19°, which is not a problem at higher energies (lower wavelengths) but may limit the applicability at energies lower than 10 keV (larger θ region required). The examples further confirm the cell's capability for various gas atmospheres as well as for liquid-phase reactions. Throughout all case studies, the cell was combined either with on-line mass spectrometric analysis in gas-phase reactions or on-line infrared spectroscopy in liquid-phase reactions. Since the geometry is similar to a plug-flow reactor, the spectroscopic cell allows experiments to be performed under realistic catalytic conditions as required for *in situ* (often also called '*operando*') studies. These features make the spectroscopic cell very flexible for studies on model systems and real catalysts, in transmission and fluorescence modes, on catalysts in the liquid and gas phase, and, finally, combination of different X-ray-based techniques.

We thank the synchrotron facilities ANKA (Forschungszentrum Karlsruhe, Germany), HASYLAB at DESY (Hamburg, Germany) and the Swiss Norwegian Beamlines at ESRF (Grenoble, France) for beam time. Stefan Mangold (ANKA-XAS), Hermann Emerich and Wouter van Beek (SNBL at ESRF), and Julia Wienold, Carsten Baehtz and Adam Webb (HASYLAB) are acknowledged for discussions and their assistance during the beam time. Furthermore, we are grateful to the European Community, Research Infrastructure Action under the FP6 'Structuring the European Research Area' program (through the Integrated Infrastructure Initiative 'Integrating Activity on Synchrotron and Free Electron Laser Science', Contract RII3-CT-2004-506008) for financial support of our measurements at ANKA and HASYLAB. We thank Niels van Vegten (ETH Zurich) for the support in preparing the noble metal catalyst samples. MC is grateful for financial support by Umicore AG (Hanau, Germany). Finally, Max Wohlwend and Roland Mäder (ETH Zurich) are acknowledged for their assistance in building up the *in situ* cell.

References

Abad, A., Concepcion, P., Corma, A. & Garcia, H. (2005). *Angew. Chem. Int. Ed.* **44**, 4066–4069.
Anderson, J. A., Bachiller-Baeza, B. & Fernández-García, M. (2003). *Phys. Chem. Chem. Phys.* **5**, 4418–4427.
Bare, S. R., Yang, N., Kelly, S. D., Mickelson, G. E. & Modica, F. S. (2007). *Catal. Today*. In the press. [doi:10.1016/j.cattod.2006.10.007.]
Barsan, N., Koziej, D. & Weimar, U. (2007). *Sens. Actuators B Chem.* **121**, 18–35.

Bazin, D., Lynch, J. & Ramos-Fernandez, M. (2003). *Oil Gas Sci. Technol.* **58**, 667–683.
Bond, G. C. & Thompson, D. T. (1999). *Catal. Rev. Sci. Eng.* **41**, 319–388.
Casapu, M., Grunwaldt, J.-D., Maciejewski, M., Baiker, A., Wittrock, M., Göbel, U. & Eckhoff, S. (2007). *Topics Catal.* In the press.
Casapu, M., Grunwaldt, J.-D., Maciejewski, M., Wittrock, M., Göbel, U. & Baiker, A. (2006). *Appl. Catal. B*, **63**, 232–242.
Chiarello, G. L., Grunwaldt, J.-D., Ferri, D., Krumeich, F., Oliva, C., Forni, L. & Baiker, A. (2007). In preparation.
Clausen, B. S., Steffensen, G., Fabius, B., Villadsen, J., Feidenhans'l, R. & Topsøe, H. (1991). *J. Catal.* **132**, 524–535.
Clausen, B. S. & Topsøe, H. (1991). *Catal. Today*, **9**, 189–196.
Clausen, B. S., Topsøe, H. & Frahm, R. (1998). *Adv. Catal.* **42**, 315–344.
Dalla Betta, R. A., Boudart, M., Foger, K., Löffler, D. G. & Sánchez-Arrieta, J. (1984). *Rev. Sci. Instrum.* **55**, 1910–1913.
Dent, A. J., Wells, M. P., Farrow, R. C., Ramsdale, C. A., Derbyshire, G. E., Greaves, G. N., Couves, J. W. & Thomas, J. M. (1992). *Rev. Sci. Instrum.* **63**, 903–906.
Engelmann-Pirez, M., Granger, P. & Leclercq, G. (2005). *Catal. Today*, **107**, 315–322.
Girardon, J.-S., Khodakov, A. Y., Capron, M., Cristol, S., Dujardin, C., Dhainaut, F., Nikitenko, S., Meneau, F., Brass, W. & Payen, E. (2005). *J. Synchrotron Rad.* **12**, 680–684.
Grunwaldt, J.-D. & Baiker, A. (2007). *AIP Conf. Proc.* **882**, 577–581.
Grunwaldt, J.-D., Caravati, M. & Baiker, A. (2006). *J. Phys. Chem. Lett. B*, **110**, 25586–25589.
Grunwaldt, J.-D., Caravati, M., Hannemann, S. & Baiker, A. (2004). *Phys. Chem. Chem. Phys.* **6**, 3037–3047.
Grunwaldt, J.-D. & Clausen, B. S. (2002). *Topics Catal.* **18**, 37–42.
Grunwaldt, J.-D., Hannemann, S., Göttlicher, J., Mangold, S., Denecke, M. A. & Baiker, A. (2005). *Phys. Scr.* T**115**, 769–772.
Grunwaldt, J.-D., Keresszegi, C., Mallat, T. & Baiker, A. (2003). *J. Catal.* **213**, 291–295.
Haider, P., Grunwaldt, J.-D. & Baiker, A. (2007). In preparation.
Hammersley, A. P. (2007). *Fit2D*, http://www.esrf.eu/computing/scientific/FIT2D/.
Hammersley, A. P., Svensson, S. O. & Thompson, A. (1994). *Nucl. Instrum. Methods A*, **346**, 312–321.
Hannemann, S., Grunwaldt, J.-D., Günther, D., Krumeich, F., Lienemann, P. & Baiker, A. (2007). *Appl. Catal. A*, **316**, 226–239.
Hannemann, S., Grunwaldt, J.-D., Krumeich, F., Kappen, P. & Baiker, A. (2006). *Appl. Surf. Sci.* **252**, 7862–7873.
Haruta, M. & Daté, M. (2001). *Appl. Catal. A*, **222**, 427–437.
Huwe, H. & Fröba, M. (2004). *J. Synchrotron Rad.* **11**, 363–365.
Iwasawa, Y. (1996). *X-ray Absorption Fine Structure for Catalysts and Surfaces.* Singapore: World Scientific.
Kampers, F. W. H., Maas, T. M. J., van Grondelle, J., Brinkgreve, P. & Koningsberger, D. C. (1989). *Rev. Sci. Instrum.* **60**, 2635–2638.
Kappen, P., Tröger, L., Materlik, G., Reckleben, C., Hansen, K., Grunwaldt, J.-D. & Clausen, B. S. (2002). *J. Synchrotron Rad.* **9**, 246–253.
Keresszegi, C., Grunwaldt, J.-D., Mallat, T. & Baiker, A. (2003). *Chem. Commun.* pp. 2304–2305.
Kucharczyk, B. & Tylus, W. (2004). *Catal. Today*, **90**, 121–126.
Longo, A., Balerna, A., d'Acapito, F., D'Anca, F., Giannici, F., Liotta, L., Pantaleo, G. & Martorana, A. (2005). *J. Synchrotron Rad.* **12**, 499–505.
Lytle, F. W., Greegor, R. B., Marques, E. C., Sandstrom, D. R., Via, G. H. & Sinfelt, J. H. (1985). *J. Catal.* **95**, 546–557.
McBreen, J. & Mukerjee, S. (1995). *J. Electrochem. Soc.* **142**, 3399–3433.
Meitzner, G. & Iglesia, E. (1999). *Catal. Today*, **53**, 433–441.
Newton, M. A., Dent, A. J. & Evans, J. (2002). *Chem. Soc. Rev.* **31**, 83–85.
Onal, Y., Schimpf, S. & Claus, P. (2004). *J. Catal.* **223**, 122–133.
Pettiti, I., Gazzoli, D., Inversi, M., Valigi, M., deRossi, S., Ferraris, G., Porta, P. & Colonna, S. (1999). *J. Synchrotron Rad.* **6**, 1120–1124.
Ressler, T. (1998). *J. Synchrotron Rad.* **5**, 118–122.
Ressler, T., Jentoft, R. E., Wienold, J., Girgsdies, F., Neisius, T. & Timpe, O. (2003). *Nucl. Instrum. Methods Phys. Res. B*, **200**, 165–170.
Revel, R., Bazin, D., Seigneurin, A., Barthe, P., Dubuisson, J. M., Decamps, T., Sonneville, H., Poher, J. J., Maire, F. & Lefrancois, P. (1999). *Nucl. Instrum. Methods Phys. Res. B*, **155**, 183–188.
Rohr, M., Günther, M., Jutz, F., Grunwaldt, J.-D., Emerich, H., van Beek, W. & Baiker, A. (2005). *Appl. Catal. A*, **296**, 238–250.
Ruban, A. V., Skriver, H. L. & Nørskov, J. K. (1999). *Phys. Rev. B*, **59**, 15990–16000.
Russell, A. E. & Rose, A. (2004). *Chem. Rev.* **104**, 4613–4635.
Stark, W. J., Grunwaldt, J.-D., Maciejewski, M., Pratsinis, S. E. & Baiker, A. (2005). *Chem. Mater.* **17**, 3352–3358.
Strobel, R., Baiker, A. & Pratsinis, S. E. (2006). *Adv. Powder Technol.* **17**, 457–480.
Strobel, R., Grunwaldt, J.-D., Camenzind, A., Pratsinis, S. E. & Baiker, A. (2005). *Catal. Lett.* **104**, 9–16.
Thomas, J. M. & Sankar, G. (2001). *J. Synchrotron Rad.* **8**, 55–60.
Topsøe, H. (2003). *J. Catal.* **216**, 155–164.
Zabinsky, S. I., Rehr, J. J., Ankudinov, A., Albers, R. C. & Eller, M. J. (1995). *Phys. Rev. B*, **52**, 2995–3009.